nature nanotechnology

ARTICLES

PUBLISHED ONLINE: 24 JULY 2011 | DOI: 10.1038/NNANO.2011.103

Electrically tuned spin–orbit interaction in an InAs self-assembled quantum dot

Y. Kanai[1†], R. S. Deacon[1,2†*], S. Takahashi[1], A. Oiwa[1,2], K. Yoshida[1], K. Shibata[3], K. Hirakawa[2,3,4], Y. Tokura[5] and S. Tarucha[1,4,6]

Electrical control over electron spin is a prerequisite for spintronics spin-based quantum information processing. In particular, control over the interaction between the orbital motion and the spin state of electrons would be valuable, because this interaction influences spin relaxation and dephasing. Electric fields have been used to tune the strength of the spin–orbit interaction in two-dimensional electron gases, but not, so far, in quantum dots. Here, we demonstrate that electrical gating can be used to vary the energy of the spin–orbit interaction in the range 50–150 μeV while maintaining the electron occupation of a single self-assembled InAs quantum dot. We determine the spin–orbit interaction energy by observing the splitting of Kondo effect features at high magnetic fields.

The spin–orbit interaction (SOI) couples the orbital motion of electrons with the spin state, providing a route towards all-electrical manipulation of electron spins, such as that proposed in the Datta-Das spin transistor[1] and spin qubits[2–5]. In two-dimensional electron gases it has been shown that the strength of the Rashba SOI is tuned by applying an electric field to alter the anisotropy of the quantum well confinement[6,7]. This effect has been harnessed to manipulate spin relaxation[8,9]. Electrical tuning of the SOI has not been demonstrated in commonly studied gate-defined GaAs quantum dots (QDs) and may require specific QD systems with a strong SOI. Recently, high-resolution electron-beam lithography techniques have allowed the contacting of single uncapped self-assembled QDs, grown by the Stranski–Krastanov mode, with source and drain electrodes[10–13]. So far, most studies focus on self-assembled InAs QDs[10,11,14,15], which exhibit strong SOI[16] suitable for fast spin manipulation[5]. For self-assembled QDs with relatively large size it was recently shown that the lateral confinement potential may be efficiently tuned using anisotropic side-gate electrodes[15], providing a method of tuning device parameters such as the tunnel coupling with the leads. In this Article, we quantitatively evaluate the SOI energy using the high-magnetic-field Kondo effect and show that electrical gating of an InAs self-assembled QD allows tuning of the SOI energy over a wide range.

Device characterization

Measurements were performed on an uncapped single InAs self-assembled QD contacted with titanium/aluminium (5/100 nm) source–drain electrodes (source–drain bias, V_{sd}) and electrically gated with both a buried back-gate (V_G) and a lateral side-gate electrode (V_{sg}). First, we study the ground-state spectrum of the QD by plotting the differential conductance ($G = dI/dV_{sd}$) as a function of V_{bg} with $V_{sd} = 0$ V (Fig. 1). Tuning a gate voltage moves the energy levels of the QD relative to the chemical potential of the leads. Peaks in the differential conductance (Coulomb peaks) occur when an energy level crosses the lead chemical potential. When no energy level is aligned with the leads, the QD is Coulomb blockaded and the conductance is suppressed[17]. Figure 1a shows the magnetic evolution of Coulomb peaks with a B-field applied perpendicular to the sample surface. The magnetic evolution reflects the electrostatic confinement, charging energy and Zeeman splitting of the discrete energy levels of the QD, which generate a wide variety of crossings. The back-gate lever arm that relates the QD energy levels to the back-gate voltage (see Supplementary Information for additional experimental data) is evaluated as $\alpha \approx 0.08 \pm 0.01$ eV V^{-1}. Typical single electron charging energies are in the range $U \approx 1.4$–2.7 meV, with energy level spacings in the range $\epsilon_d \approx 0.3$–0.7 meV. As a consequence of the selection of a relatively large QD, we were unable to reach the single electron regime, and in region III the device is occupied by at least 20 electrons. A large QD has the advantage that the side-gate may more effectively manipulate the wavefunctions due to weaker lateral confinement. Study of the spectrum of Coulomb peaks at low magnetic fields ($B < 1$ T) shows a clear signature of even/odd electron occupation and the spin-1/2 Kondo effect (see Supplementary Information), from which we determine that region II has an odd electron number and regions I/III have even electron numbers. The Landé g-factor evaluated for low B-field data in various charge states (V_G regions) varies non-systematically over a wide range from $g \approx 2.3$ to 11.8 depending on the charge state of the QD (see Supplementary Information) and is similar to the large variations recently reported for InAs[18] and InSb[19,20] nanowire QD devices. For the lowest $|g|$ evaluated from low B-field data we find that the Zeeman energy exceeds the orbital energy for $B > 5$ T. For high B-fields Zeeman-induced transitions in the ground-state therefore dominate.

Evaluation of SOI energy

When two different orbital states ($|a\rangle$ and $|b\rangle$) with opposite spin are tuned to a degeneracy, the SOI hybridization causes an avoided crossing in the energy spectrum with a width that is twice the SOI energy (Δ), as shown schematically in Fig. 1b. In small QDs this hybridization energy cannot be measured precisely in the ground-state spectrum (such as Fig. 1a), because the single electron charging

[1]Department of Applied Physics, University of Tokyo, 7-3-1 Hongo, Bunkyo-ku, 113-8656, Japan, [2]JST CREST, 4-1-8 Hon-cho, Kawaguchi-shi, Saitama 332-0012, Japan, [3]Institute of Industrial Science, University of Tokyo, 4-6-1 Komaba, Meguro-ku, Tokyo 153-8505, Japan, [4]INQIE, University of Tokyo, 4-6-1 Komaba, Meguro-ku, Tokyo 153-8505, Japan, [5]NTT Basic Research Laboratories, NTT Corporation, Atsugi-shi, Kanagawa, 243-0198, Japan, [6]QPEC, University of Tokyo, 7-3-1 Hongo, Bunkyo-ku, Tokyo 113-8656, Japan; †These authors contributed equally to this work. *e-mail: russell@meso.t.u-tokyo.ac.jp

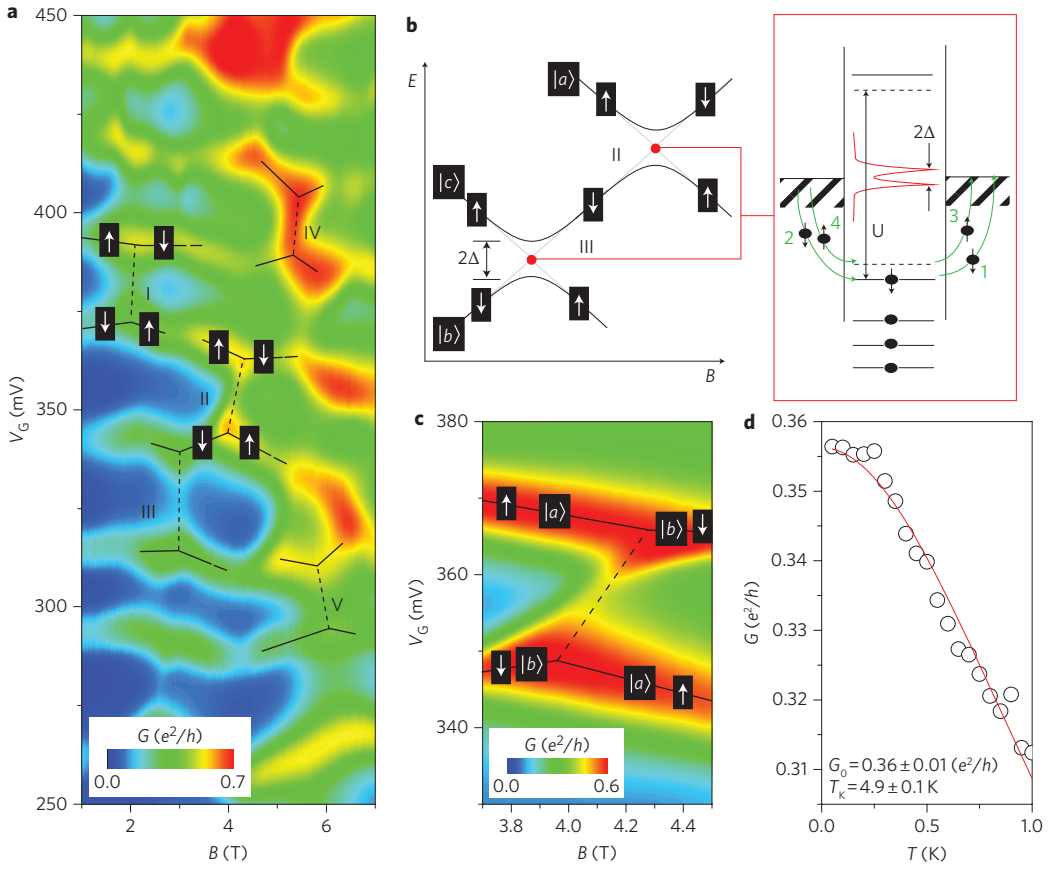

Figure 1 | Magnetic evolution of system ground states. a, False-colour plot of differential conductance ($G = dI/dV_{sd}$), showing the magnetic evolution of the Coulomb charging peaks for $V_{sd} = 0$ V and $V_{sg} = -0.5$ V. The external magnetic field is applied out-of-plane, $\mathbf{B}_{ext} \| z$. Solid lines are a guide to the eye indicating spin-up (↑) and spin-down (↓) electron states that create the crossings in regions I, II and III. **b**, Schematic representation of the energy levels for two crossings (equivalent to II and III). In each case, two single-particle energy levels with different orbital and opposite spin states are tuned to a degeneracy at which the SOI hybridization occurs. The resulting avoided crossing may be detected as a splitting of the high B-field Kondo feature, which is possible wherever there is a degeneracy of two opposite spin states. Green arrows indicate a fourth-order tunnelling process, which is representative of the high-order processes that generate the Kondo feature. The Kondo peak at the Fermi energy is split due to the hybridization of the crossing levels. **c**, False-colour plot of $G(V_G, B)$ about region II with $V_{sd} = 0$ mV and $V_{sg} = -0.5$ V. **d**, Differential conductance at the centre of region II (half-filling condition) for $V_{sd} = 0$ mV as a function of temperature. The red line indicates a best fit using the empirical expression discussed in the text.

energy U typically significantly exceeds Δ. A more direct measurement of the local density of states is achieved by measuring the differential conductance as a function of V_{sd}. The local energy levels (ground states and excited states) may then be directly probed by electrons tunnelling from the chemical potential of the leads; however, a small tunnel coupling is required to resolve the excited and ground states. At high magnetic fields, the Kondo effect occurs in our device wherever there are two degenerate states with different spins, regardless of the occupation of the QD. If the SOI-induced hybridization at the crossing is sizeable, the degeneracy of the states is lifted and the Kondo feature is split into two peaks. A similar splitting is observed when a large magnetic field lifts the degeneracy[21]. The splitting of the Kondo feature provides a direct measure of the SOI and is equivalent to the excited-state spectroscopy used elsewhere[16,19,22]. We focus on the crossing in region II, which is shown in detail for $V_{sg} = -0.5$ V in Fig. 1c. The selection of a large QD complicates the assignment of orbital angular momentum quantum numbers, but the spin component of the wavefunctions is well characterized and indicates that $|a\rangle$ and $|b\rangle$ are eigenstates with opposite spin. When the magnetic field tunes the two states to a degeneracy, the conduction electrons in the leads may coherently screen the unpaired electron spin on the QD through Kondo spin-flip co-tunnelling processes, giving rise to the Kondo effect[14,23]. The resulting dynamic singlet state lifts the Coulomb blockade, enhancing the conductance as observed along the dashed line in Fig. 1c. The energy level spacing is sufficiently large that we may consider the Kondo state equivalent to the conventional SU(2) spin-1/2 case. The Kondo effect is confirmed through observation of a decrease of the peak conductance of the zero-bias anomaly with increasing temperature (Fig. 1d). From the peak conductance we extract a rough estimate of the Kondo temperature using the empirical expression[24–26] $G(T) = G_0/[1 + (2^{1/s} - 1)(T/T_K)^2]^s$, where G_0 is the $T = 0$ K conductance and $s = 0.21$ for a spin-1/2 system. Best fits indicate that $T_K \approx 4.9 \pm 0.5$ K. Interestingly, the Kondo feature is observed to move to higher magnetic fields for larger V_G, indicating that V_G may lift the degeneracy of the two orbital states, and a larger B-field is then required to tune the system back to the degenerated point. This we attribute to the sensitivity of the specific orbital states to the confinement potential of the QD. Note that other crossings with both even and odd electron occupation, such as regions I, III, IV and V in Fig. 1a, also display the Kondo effect and show a similar (albeit weaker) and/or opposite dependence on V_G.

Electrical tunability of the SOI energy

Careful examination of the Kondo region indicates that for some side/back-gate conditions the Kondo feature is split, indicating that the degeneracy is lifted through SOI-induced hybridization.

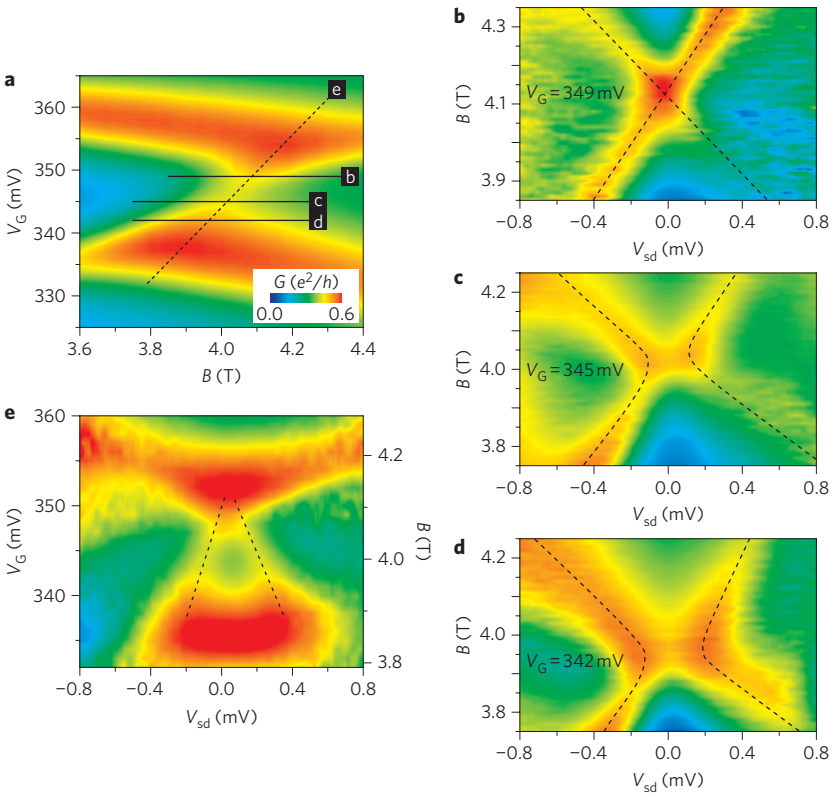

Figure 2 | Hybridization of the orbital states. a, False-colour $G(V_G, B)$ plot focusing on region II, with $V_{sd} = 0$ V and $V_{sg} = 0$ V. Solid and dashed lines indicate the ranges of V_G and B swept in measurements **b**–**d** and **e**, respectively. All measurements are plotted with the same colour scale (units of e^2/h) as in **a**. Dashed lines in **b**–**e** indicate the split Kondo feature.

Example transport measurements are shown in Fig. 2 for $V_{sg} = 0$ V. Figure 2b–d displays non-equilibrium transport measurements of the Kondo feature at different values of V_G, corresponding to the horizontal solid lines in Fig. 2a. Note that even in the absence of SOI the degeneracy may appear to be lifted as a function of magnetic field, V_G or V_{sg}. In the present measurement we systematically scan the parameter space (examples in Fig. 2b–d) to confirm that an avoided crossing occurs and degeneracy is lifted for all values of B, V_G and V_{sg}. We can therefore rule out the possibility that we have measured away from the most degenerated condition. Measurements in Fig. 2b–d are well reproduced by taking data along the diagonal dashed line in Fig. 2a to observe the Kondo feature at the most degenerated conditions (Fig. 2e). As we consider the crossing of two states with opposite spin, the avoided crossing is attributed to the SOI. This conclusion is supported by the observation of strong SOI anisotropy when the magnetic field is applied for different in-plane directions, which will be discussed later. The avoided crossing in the energy spectrum has a width of 2Δ and is observed as two peaks at $eV_{sd} = \pm 2\Delta$.

We now consider the effect of the side-gate on SOI hybridization. Figure 3a displays the position of Coulomb charging peaks as a function of V_G and B for a range of V_{sg}. A small change in the local electrostatic environment, probably caused by the charging of a nearby QD, shifts the position of charging resonances compared with those seen in Figs 1 and 2. Despite this shift, the relative values of V_G required to charge the device remain the same. Tuning the QD chemical potential by increasing V_{sg} shifts the charging peaks to lower V_G and also reduces the B-field required to observe the degenerated condition. Following the technique used to examine the anti-crossing of states in Fig. 2e, we tune both V_G and B to maintain the most degenerated condition and sweep V_{sd} (measuring along the dashed lines in Fig. 3a). Each measurement is again carefully checked to ensure the most degenerated condition is measured as previously shown in Fig. 2b–d. Results for a range of values of V_{sg} are plotted in Fig. 3b–d. As V_{sg} is increased, we observe an increase in the splitting of the Kondo feature and that the dependence of this splitting on V_G is reduced until at $V_{sg} \approx +1.0$ V no V_G dependence is observed.

The use of both side-gate and back-gate allows the tuning of the confinement potential while maintaining the charge state of the QD. Figure 3e compares the Kondo zero-bias anomaly at the half-filling condition in region II for a range of V_{sg}. We note that the inelastic co-tunnelling process does not significantly contribute to the splitting of the Kondo feature in the V_{sg} range studied, as the half width of the splitting is less than the Kondo temperature. In Fig. 4, we evaluate and plot Δ as a function of V_{sg} at the half-filling condition. In region II, Δ is tuned between 50 μeV and 150 μeV. Further tuning was impossible due to leakage of the side-gate electrode. Using similar analysis as that in region II we study regions IV and V (Fig. 1a) and evaluate Δ at half-filling in the centre of the Kondo region. In contrast to region II, we note that in region IV, V_{sg} has a negligible effect on Δ. This result indicates that the effect of V_{sg} (and V_G) varies with the specific orbital states.

In-plane anisotropy of the SOI energy

In the present measurement we are unable to discriminate the contributions from Rashba or Dresselhaus spin–orbit terms based on known selection rules[16] due to the unknown orbital states. We note, however, that a previous experiment on the two-electron state in a similar InAs self-assembled QD[16] found a Rashba-induced spin–orbit energy of $\Delta \approx 150$ μeV. It is also known that the Dresselhaus term is typically smaller than the Rashba in narrow-gap QDs[27]. As the measured hybridization energy is similar to the previously measured Rashba SOI energy, it is reasonable to assume that the Rashba term is dominant

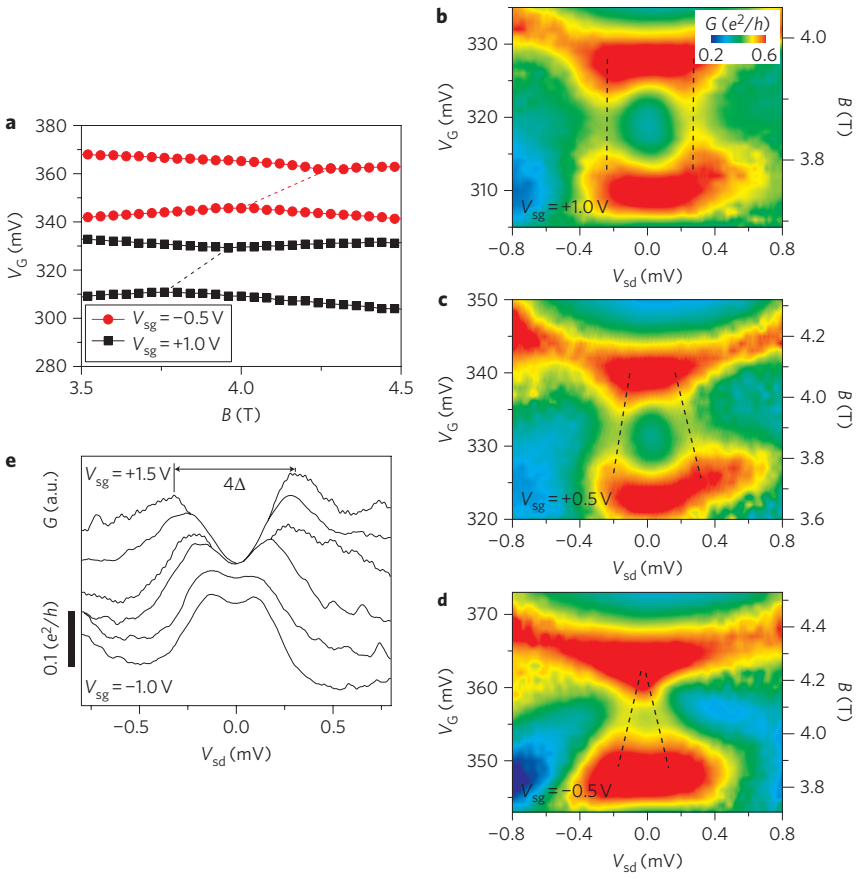

Figure 3 | Action of the side-gate. a, Positions of the Coulomb charging resonances for $V_{sd} = 0$ V. Dashed lines indicate the position of the degenerated crossing/anti-crossing point. **b–d**, False-colour plots of differential conductance collected by sweeping V_{sd} while simultaneously stepping both B and V_G to follow the dashed lines in **a**. **e**, $G(V_{sd})$ traces at the half-filling condition in the centre of region II for a range of V_{sg}. Traces are offset for clarity.

in our case. The SOI hybridization is then given by $\Delta = |\langle a\uparrow|\mathcal{H}_{SOI}|b\downarrow\rangle| = |\langle a\uparrow|\lambda\mathbf{E}\cdot(\mathbf{p}\times\boldsymbol{\sigma})|b\downarrow\rangle|$, where λ is the SOI parameter, $\mathbf{p}$ is the electron momentum, $\mathbf{E}$ is the electric field and $\boldsymbol{\sigma}$ is the Pauli matrix vector. A complex transition vector for the momentum may be defined as $\mathbf{Q} = \langle a|\mathbf{p}|b\rangle$. The effective SOI magnetic field acting on the spin is then $\mathbf{B}_{SOI} = \lambda\mathbf{E}\times\mathbf{Q}$. (Note that the effective SOI magnetic field in a QD, which is a complex vector, has less physical meaning than in the extended system, where it is a well-defined internal magnetic field pointing normal to the electric field as well as to the momentum; see Supplementary Information for additional details.) The SOI energy Δ is determined by the outer product of $\mathbf{B}_{SOI}$ and a vector parallel to the applied external magnetic field ($\mathbf{B}_{ext}$). When $\mathbf{B}_{ext}$ is applied at a 'magic angle', parallel to the real vector $\mathbf{B}_{SOI}/i$, the SOI is quenched and no avoided crossing is observed[16] (see Supplementary Information for additional details).

From consideration of the geometry of the QD measured in this Article, we would expect strong out-of-plane confinement resulting in $\mathbf{B}_{SOI}$ with a large, possibly dominant, in-plane component[16]. To test the in-plane anisotropy of Δ we remeasured the device using a single axis rotator with the magnetic field set in-plane and perpendicular to the QD electrodes taken as $\theta = 0 \pm 1^\circ$ (Fig. 5b). A plot of the evolution of Coulomb charging peaks with magnetic field for $V_{sg} = -0.5$ V, $\theta = -20^\circ$ and $V_{sd} = 0$ mV is shown in Fig. 5a. The thermal cycle of the device changed the spectrum of Coulomb charging peaks and (anti-)crossings, but we were able to reproduce similar split peak Kondo features, indicating the hybridization of two orbital states. In this case we focus on the crossing indicated by the dashed line in Fig. 5a, where the QD is occupied by an even number of electrons. Figure 5c shows Δ as a function of θ for $V_{sg} = -0.5$ V and $V_{sg} = 1.0$ V. When the device is rotated we observe that Δ for both traces is a minimum around $\theta \approx -30^\circ$, but away from this θ, the two traces are not equal, indicating that Δ is electrically tunable. Following our previous study[16], we fit the data using $\Delta = A|\cos(\theta - \theta_0)| + B$, where A, B and θ_0 are free fitting parameters. The constant offset B accounts for the lack of quenching of Δ and θ_0 indicates the in-plane offset of the real vector $\mathbf{B}_{SOI}/i$. Best fits indicate $\theta_0 \approx 60 \pm 4^\circ$ and $\theta_0 \approx -51 \pm 5^\circ$ for $V_{sg} = -0.5$ V and $V_{sg} = 1.0$ V, respectively. The cosine-like dependence of Δ on θ supports the attribution of the observed avoided crossings to Rashba SOI. The offset of $\theta_0 \approx 30^\circ$ reflects the electrostatic confinement and relative orientation/position of the wavefunctions $|a\rangle$ and $|b\rangle$.

We expect the dominant confinement field component to be out-of-plane and very large compared with the small perturbation applied by the side-gate electrode, so it is unlikely that changes in $|\mathbf{E}|$ account for the tuning of Δ. Another possibility is that changes in lateral confinement affect the energy level spacing, changing the overlap integral of $|a\rangle$ and $|b\rangle$ and resulting in a change of $|\mathbf{B}_{SOI}|$. Analysis of the V_{bg} separations of Coulomb peaks at low magnetic fields indicates that changes in the energy level spacing do not exceed 20% of the maximum over the full V_{sg} range studied (see Supplementary Information). This small variation again seems unlikely to account alone for the large variation of Δ observed in the experiment. Considering the experimental observations, we propose a mechanism for the tunable SOI observed in this report based on manipulation of the relative position of the orbital wavefunctions, which alters $\mathbf{B}_{SOI}$. First consider the case of a two-dimensional QD. Here $\mathbf{E}$ may be considered to have only an out-of-plane component and $\mathbf{p}$ for the states lies in-plane,

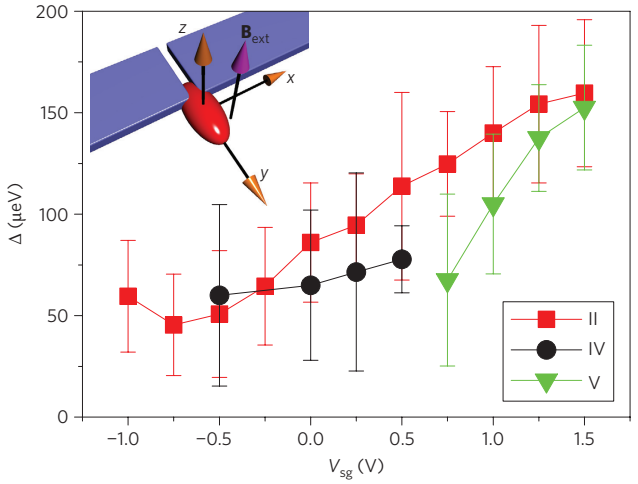

Figure 4 | Electrical control of SOI. Plot of SOI hybridization energy evaluated in the centre of regions II, IV and V for a range of V_{sg}. Bars indicate a quarter of the full-width at half-maximum of the peaks for comparison. Inset: schematic of the device with relevant axes indicated. Source and drain electrodes are indicated in blue, with the QD drawn in red as an elongated semi-ellipsoid. The external magnetic field is applied out-of-plane, $\mathbf{B}_{ext} \| z$.

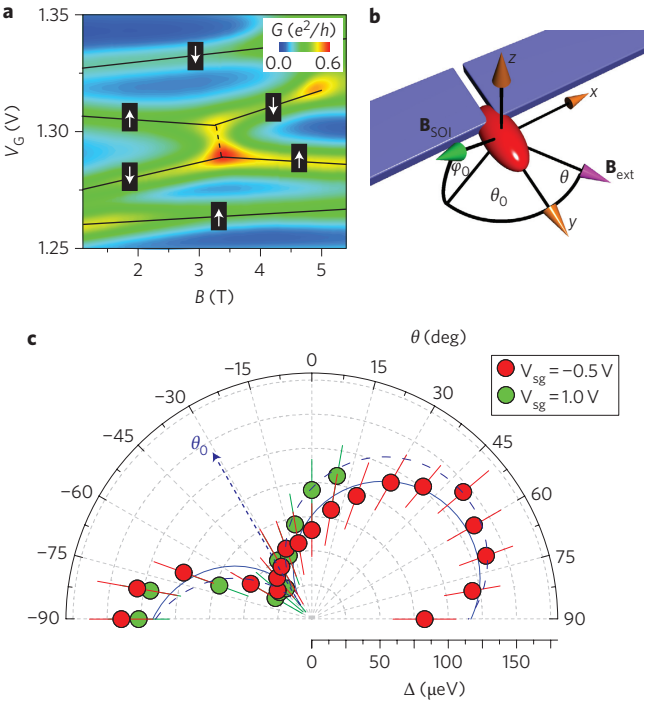

Figure 5 | Azimuthal B-field rotation. a, False-colour plot of $G(V_G, B)$ for $V_{sd} = 0$ V, $V_{sg} = -0.5$ V and $\theta = -20°$. **b**, Schematic of the device with relevant axes indicated. The external field $\mathbf{B}_{ext}$ is applied in-plane with angle θ measured from the y-axis. **c**, SOI energy Δ as a function of θ for $V_{sg} = -0.5$ V and $V_{sg} = 1.0$ V. Bars indicate a quarter of the full-width at half-maximum of the split peaks for comparison. The solid (dashed) blue line indicates an absolute cosine function fit to the $V_{sg} = 0$ V (-0.5 V) data, as described in the main text. The blue dashed arrow shows the approximate in-plane direction of the real vector $\mathbf{B}_{SOI}/i$ indicated by the offset angle of the cosine fit, θ_0.

resulting in a $\mathbf{B}_{SOI}$ that is always in the plane of the surface. In this case we expect quenching of Δ when $\mathbf{B}_{ext}$ is applied for some in-plane vector[16] parallel with $\mathbf{B}_{SOI}$. One possible method of tuning $\mathbf{B}_{SOI}$ is a relative displacement of wavefunctions $|a\rangle$ and $|b\rangle$, which may occur when the confinement potential is perturbed. Such tuning may change the in-plane direction of $\mathbf{B}_{SOI}$ and subsequently the 'magic angle' at which an in-plane $\mathbf{B}_{ext}$ may quench Δ. This may then lead to a tunable Δ, but only when $\mathbf{B}_{ext}$ is applied in-plane. For the two-dimensional QD in an out-of-plane magnetic field ($\mathbf{B}_{ext} \| \mathbf{E}$), the observed Δ will always be a maximum, and no quenching/tunability of Δ would be observed for side-gate modulation. However, if we consider a QD with a three-dimensional confinement the situation is different. As the states may now have some out-of-plane momentum and the electric field can no longer be considered to have only an out-of-plane component, $\mathbf{B}_{SOI}$ is no longer confined in-plane, but is tilted out-of-plane as illustrated in Fig. 5b. Here, relative displacement of the wavefunctions $|a\rangle$ and $|b\rangle$ may affect both the in-plane angle (θ_0) of $\mathbf{B}_{SOI}$, and the out-of-plane angle (ϕ_0), leading to tunability for both in-plane and out-of-plane magnetic fields. The lack of quenching of Δ observed in the experiment (Fig. 5c) is a strong indication that the system may not be considered to be simply two-dimensional, as an in-plane $\mathbf{B}_{ext}$ is insufficient to quench Δ and full three-axis vector control of the magnetic field would be required to achieve the quenching condition. In Fig. 5c, we observe a shift in θ_0, indicating that V_{sg} has an influence on the direction of $\mathbf{B}_{SOI}$. From this, and based on the arguments above, we propose that V_{sg} strongly influences the relative lateral position of wavefunctions $|a\rangle$ and $|b\rangle$. Note also that similar arguments are made for previously reported electrical tunability of the tunnel coupling with the source–drain leads[15].

In summary, we have studied the SOI in a single InAs self-assembled QD device through observation of the splitting of high B-field Kondo features. We have observed that electrostatic gating of the device allows tuning of the SOI. The gates allow alteration of the QD confinement potential, which influences the wavefunctions and allows the SOI to be influenced. Further studies will be required to elucidate the effect of V_{sg} on the SOI 'magic angle'.

Methods. Measurements were performed on a single InAs self-assembled QD grown by means of the Stranski–Krastanov mode. Nanogap electrodes were fabricated using electron-beam lithography and electron-beam evaporation to pattern and deposit a bilayer comprising 5 nm titanium and 100 nm aluminium. Before deposition of the nanogap, the QD was etched in 40% buffered hydrofluoric acid to improve the transparency of the resulting contacts. Further details of the device fabrication technique may be found in ref. 10. The QD studied had an elongated, approximately elliptical shape with nominal physical dimensions $d_x \approx$ 100 nm, $d_y \approx 200$ nm and a height of ~15 nm, where in-plane axes x and y were parallel and perpendicular to the leads respectively (see Supplementary Information for additional device details). Measurements were performed in a He^3–He^4 dilution refrigerator with base temperature of 35 mK using conventional lock-in techniques and an a.c. excitation of 3 μV. Measurements of the in-plane anisotropy of the SOI were conducted using a single-axis rotation gear mounted on the dilution refrigerator mixing chamber, which allowed control of the rotation to an accuracy of $\pm 1°$. Note that at low temperatures and magnetic fields the device source and drain electrodes are superconducting[15]. The critical out-of-plane magnetic field required to drive the leads into the normal state at the base temperature of the dilution refrigerator was $B_c \approx 150$ mT. As the study in this report is concerned with features observed at high $B \gg B_c$, superconducting transport has no relevance to the physics discussed.

Received 20 January 2011; accepted 2 June 2011;
published online 24 July 2011

References

1. Datta, S. & Das, B. Electronic analog of the electro-optical modulator. *Appl. Phys. Lett.* **56,** 665–667 (1990).
2. Rashba, E. & Efros, A. Orbital mechanisms of electron-spin manipulation by an electric field. *Phys. Rev. Lett.* **91,** 126405 (2003).
3. Golovach, V., Borhani, M. & Loss, D. Electric-dipole induced spin resonance in quantum dots. *Phys. Rev. B* **74,** 165319 (2006).
4. Nowack, K., Koppens, F., Nazarov, Y. & Vandersypen, L. Coherent control of a single electron spin with electric fields. *Science* **318,** 1430–1433 (2007).

5. Nadj-Perge, S., Frolov, S., Bakkers, E. & Kouwenhoven, L. Spin–orbit qubit in a semiconductor nanowire. *Nature* **468,** 1084–1087 (2010).
6. Studer, M., Salis, G., Ensslin, K., Driscoll, D. & Gossard, A. Gate-controlled spin–orbit interaction in a parabolic GaAs/AlGaAs quantum well. *Phys. Rev. Lett.* **103,** 027201 (2009).
7. Nitta, J., Akazaki, T., Takayanagi, H. & Enoki, T. Gate control of spin–orbit interaction in an inverted $In_{0.53}Ga_{0.47}As/In_{0.52}Al_{0.48}As$ heterostructure. *Phys. Rev. Lett.* **78,** 1335–1338 (1997).
8. Koralek, J. D. *et al.* Emergence of the persistent spin helix in semiconductor quantum wells. *Nature* **458,** 610–613 (2009).
9. Kunihashi, Y., Kohda, M. & Nitta, J. Enhancement of spin lifetime in gate-fitted InGaAs narrow wires. *Phys. Rev. Lett.* **102,** 226601 (2009).
10. Jung, M. *et al.* Lateral electron transport through single self-assembled InAs quantum dots. *Appl. Phys. Lett.* **86,** 033106 (2005).
11. Jung, M. *et al.* Shell structures in self-assembled InAs quantum dots probed by lateral electron tunneling structures. *Appl. Phys. Lett.* **87,** 203109 (2005).
12. Nakaoka, T., Kako, S., Tarucha, S. & Arakawa, Y. Coulomb blockade in a self-assembled GaN quantum dot. *Appl. Phys. Lett.* **90,** 162109 (2007).
13. Katsaros, G. *et al.* Hybrid superconductor–semiconductor devices made from self-assembled SiGe nanocrystals on silicon. *Nature Nanotech.* **5,** 458–464 (2010).
14. Igarashi, Y. *et al.* Spin-half Kondo effect in a single self-assembled InAs quantum dot with and without an applied magnetic field. *Phys. Rev. B* **76,** 081303 (2007).
15. Kanai, Y. *et al.* Electrical control of Kondo effect and superconducting transport in a side-gated InAs quantum dot Josephson junction. *Phys. Rev. B* **82,** 054512 (2010).
16. Takahashi, S. *et al.* Large anisotropy of spin–orbit interaction in a single InAs self-assembled quantum dot. *Phys. Rev. Lett.* **104,** 246801 (2010).
17. Kouwenhoven, L. *et al. Single-Electron Tunneling and Mesoscopic Devices* (Nato-Series Kluwer, 1997).
18. Csonka, S., Hofstetter, L., Freitag, F., Oberholzer, S. & Schönenberger, C. Giant fluctuations and gate control of the *g*-factor in InAs nanowire quantum dots. *Nano Lett.* **8,** 3932–3935 (2008).
19. Nilsson, H. A. *et al.* Giant level-dependent *g* factors in InSb nanowire quantum dots. *Nano Lett.* **9,** 3151–3156 (2009).
20. Nilsson, H. A. *et al.* Correlation-induced conductance suppression at level degeneracy in a quantum dot. *Phys. Rev. Lett.* **104,** 186804 (2010).
21. Meir, Y., Wingreen, N. & Lee, P. Low-temperature transport through a quantum dot: the anderson model out of equilibrium. *Phys. Rev. Lett.* **70,** 2601–2604 (1993).
22. Fasth, C., Fuhrer, A., Samuelson, L., Golovach, V. & Loss, D. Direct measurement of the spin–orbit interaction in a two-electron InAs nanowire quantum dot. *Phys. Rev. Lett.* **98,** 266801 (2007).
23. Sasaki, S., Amaha, S., Asakawa, N., Eto, M. & Tarucha, S. Enhanced Kondo effect via tuned orbital degeneracy in a spin 1/2 artificial atom. *Phys. Rev. Lett.* **93,** 017205 (2004).
24. Ng, T. K. & Lee, P. A. On-site Coulomb repulsion and resonant tunneling. *Phys. Rev. Lett.* **61,** 1768–1771 (1998).
25. Glazman, L. & Raikh, M. E. Resonant Kondo transparency of a barrier with quasilocal impurity states. *JETP Lett.* **47,** 452–455 (1988).
26. Goldhaber-Gordon, D. *et al.* From the Kondo regime to the mixed-valence regime in a single-electron transistor. *Phys. Rev. Lett.* **81,** 5225–5228 (1998).
27. Destefani, C., Ulloa, S. E. & Marques, G. Spin–orbit coupling and intrinsic spin mixing in quantum dots. *Phys. Rev. B* **69,** 125302 (2004).

Acknowledgements

The authors acknowledge discussions with R. Sakano. This work was supported by a Grant-in-Aid for Research S (no. 19104007) and A (no. 21244046), MEXT KAKENHI 'Quantum Cybernetics' project, the Strategic International Cooperative Program, DFG-JST joint research project ('Topological Electronics'), the Japan Society for the Promotion of Science (JSPS) through its Funding Program for World-Leading Innovative R&D on Science and Technology (FIRST Program), and the Special Coordination Funds for Promoting Science and Technology, MEXT (Japan). S. Tarucha acknowledges support from an IARPA grant ('Multi-Qubit Coherent Operations') through Harvard. S. Takahashi and Y.K. are supported by JSPS Research Fellowships for Young Scientists.

Author contributions

Y.K. and R.S.D. performed measurements, analysed the results and wrote the manuscript. S. Takahashi contributed to interpretation of the data. K.Y. contributed to device fabrication. K.S. and K.H. grew the self-assembled InAs quantum dot samples. Y.T. performed simulations of the system, which were crucial to interpretation of data. A.O. and S. Tarucha directed the research. All authors discussed the results and commented on the manuscript.

Additional information

The authors declare no competing financial interests. Supplementary information accompanies this paper at www.nature.com/naturenanotechnology. Reprints and permission information is available online at http://www.nature.com/reprints. Correspondence and requests for materials should be addressed to R.S.D.